JMR Journal of Meteorological Research

Joint Effect of East Asia/Pacific and Eurasian Teleconnections on the Summer Precipitation Pattern in North Asia

Po HU, Guolin FENG, Muhammad Mubashar DOGAR, Jianbo CHENG, Zhiqiang GONG

Citation: Po HU, Guolin FENG, Muhammad Mubashar DOGAR, Jianbo CHENG, Zhiqiang GONG, 2020. Joint Effect of East Asia/Pacific and Eurasian Teleconnections on the Summer Precipitation Pattern in North Asia, Journal of Meteorological Research, 34, 1–17. doi: 10.1007/s13351–020–9112–z.

View online: http://www.jos.ac.cn/article/shaid/dd9b03c271d186224acc214ae913cb993cf4430bffabf1d82226d8e6127c6376

Joint Effect of East Asia/Pacific and Eurasian Teleconnections on the Summer Precipitation Pattern in North Asia

Po HU[1], Guolin FENG[2,4], Muhammad Mubashar DOGAR[3], Jianbo CHENG[5], and Zhiqiang GONG[2*]

1 *Hubei Key Laboratory for Heavy Rain Monitoring and Warning Research, Institute of Heavy Rain, China Meteorological Administration, Wuhan* 430205, *China*

2 *National Climate Center, China Meteorological Administration, Beijing* 10081, *China*

3 *Global Change Impact Studies Centre (GSISC), Ministry of Climate Change, Islamabad* 44000, *Pakistan*

4 *College of Physical Science and Technology, Yangzhou University, Yangzhou* 225002, *China*

5 *College of Atmospheric Sciences, Lanzhou University, Lanzhou* 730000, *China*

(Received October 18, 2019; in final form February 19, 2020)

ABSTRACT

This paper focuses on the configurations of the East Asia/Pacific (EAP) and Eurasian (EU) teleconnections and their synergistic effects on summer precipitation in North Asia (NA). It is found that the configurations of the EAP and EU teleconnection anomalies reflected by EAP and EU indices can be classified into four categories: Category I (II) with consistent positive (negative) phases of EAP and EU and Category III (IV) with the EAP being a positive (negative) phase and the EU being a negative (positive) phase. Further analyses show that these four categories of EAP and EU anomalies are coherently related to different atmospheric circulations over the mid-latitude region of the EU continent, leading to different summer precipitation modes in NA. Category I (II) corresponds to a zonal triple structure of the geopotential height at 500 hPa in the region between Eastern Europe and the Sea of Japan, leading to less (more) precipitation than normal in Eastern Europe, Japan, and their surrounding areas, and more (less) precipitation in the region from Central China to Baikal Lake and eastern Russia. Category III (IV) corresponds to a meridional dipole structure of the geopotential height at 500 hPa over NA, leading to more (less) precipitation than normal in the northern part of NA and less (more) precipitation in most of the southern part of NA. In addition, the EAP teleconnection is positively correlated with the precipitation in the region between the eastern part of Baikal Lake and Okhotsk Sea and is negatively correlated with the precipitation in the region between Northeast China and Japan. Coincidently, the EU teleconnection and precipitation have negative correlations in Ural Mountain and Okhotsk Sea areas and positive correlations in the Baikal Lake area. The respective functions of EAP and EU on the summer precipitation in NA suggest that the EAP northern lobe overlapped with the central and EU eastern lobes can extend geopotential anomalies over Baikal Lake to Russian Far East, creating an EAP–EU synergistic effect on summer precipitation in NA.

Key words: teleconnection, precipitation configuration, spatial mode, synergistic effect

Citation: Hu, P., G. L. Feng, M. M. Dogar, et al., 2020: Joint effect of East Asia/Pacific and Eurasian teleconnections on the summer precipitation pattern in North Asia. *J. Meteor. Res.*, **34**(3), 1–16, doi: 10.1007/s13351-020-9112-z.

1. Introduction

While analyzing the relationship between the equatorial Pacific sea surface temperature (SST) anomaly and Northeast Pacific westerlies circulation, Bjerknes (1969) found that the winters of 1957–1958, 1963–1964, and 1965–1966 have similar correlations, which are called teleconnections. With the development of relevant studies, the correlation between the anomalous circulations over the two different regions is generally defined as the teleconnection. It has also been revealed that atmospheric teleconnection patterns play important roles in influencing global climate anomalies, which have been highly valued by many meteorologists in previous studies (Fan and Wang, 2004; Li et al., 2008; Wang et al., 2012; Grotjahn et al., 2016; Lin and Lu, 2016; Dogar et al., 2017).

Supported by the National Key Research and Development Program of China (2018YFA0606301 and 2018YFC1507702) and National Natural Science Foundation Project of China (41875100, 41575082, and 41530531).

*Corresponding author: gongzq@cma.gov.cn.

The East Asia/Pacific (EAP) teleconnection, also called the Pacific–Japan (PJ) teleconnection pattern, was first proposed by Huang and Li (1987) and Nitta (1987). When the temperature of the western Pacific warm pool is low, the weakened convective activity occurred in the Philippine and maritime area, leading to a "+ − +" EAP teleconnection pattern, with more precipitation in the Yangtze–Huaihe River Basin, Korean Peninsula, and Japanese area, and vice versa. Subsequently, the EAP index was defined based on the EAP teleconnection pattern, which has a strong relationship with the summer climate of the East Asian (EA) region, as studied in detail by Huang et al. (2004). Huang et al. (2007) revealed that the EAP meridional tripole pattern from the tropics poleward to the extra-tropics was mainly triggered by anomalies of the convective activity over the tropical western Pacific, which can be found on different time scales. Gong et al. (2017, 2018a) pointed out that the formation of the EAP pattern is closely related to the heating of the tropical western and eastern Pacific. In addition, Bueh et al. (2008) argued that the maintenance and development of the EAP teleconnection pattern is closely related to the energy that is propagated downstream through flux waves at the middle and high latitudes of the Eurasian (EU) continent. Yang et al. (2010) showed that the EAP teleconnection with the "− + − (+ − +)" pattern can promote (inhibit) the northward expansion of the Western Pacific Subtropical High (WPSH), thus affecting the northern (southern) part of the Huaihe region. Li et al. (2016) further presented the close relationship between the low-frequency oscillation of the EAP teleconnection and the persistent rainstorm in the lower reaches of the Yangtze–Huaihe River. Srinivas et al. (2018) showed that anticyclone and low-level circulation anomalies in the western Pacific region increase precipitation in southern and northern India, confirming the association between the PJ teleconnection and Indian monsoon precipitation. Wang et al. (2018) found that the EAP teleconnection has a significant relationship with the wave activity flux, which has an effect on the extreme precipitation in the middle and lower reaches of the Yangtze River under the interaction of low, medium, and high levels.

The EU teleconnection pattern is one of the five important teleconnection wave trains propagated from west to east over the EU continent. Wallace and Gutzler (1981) proposed that this is from the 500-hPa height field in the Northern Hemisphere. The EU teleconnection pattern mainly reflects the inverse correlation between the geopotential height over western Europe and Siberia, but it shows a positive correlation with Northeast China and Japan. Lee et al. (2005) found that the summer EU teleconnection is closely correlated with precipitation in the tropical region. When the EU index is positive, the surface temperature in South China is low (Zhou W. et al., 2009), and there is more rainfall in Tokyo (Tachibana et al., 2007). Barnston and Livezey (1987) studied the decomposition of EU teleconnection patterns into EU teleconnection I (EUI) and II (EUII). Liu et al. (2014) compared the spatial features, temporal variability, and difference of the winter climate among the three EU teleconnections defined by Wallace and Gutzler (1981). The EU teleconnection pattern has a significant influence on the plateau and ocean subtropical jets, which in turn affects the winter temperature and precipitation in China (Wang and Zhang, 2015). Hingmire et al. (2019) confirmed that the positive (height excess over Siberia) EU teleconnection phase favors the occurrence of widespread fog in the Indo-Gangetic region.

Previous studies have shown that the EU teleconnection has a significant impact on the climate of Eurasia, especially on the climate of EA (Wallace and Gutzler, 1981; Takaya and Nakamura, 2013; Wang and Chen, 2014). The EAP teleconnection also has a significant impact on the EA climate (Huang and Sun, 1992; Ueda et al., 1995; Nitta and Hu, 1996; Chen and Zhai, 2015). Nitta et al. (1996) showed that the variation of the summer precipitation and temperature in China are both relevant to the influence of EAP and EU patterns. The zonal teleconnection along the jet stream and the EAP teleconnection along the meridional direction are two important teleconnection lines in summer, which are interactive with each other over North Asia (NA) and EA. Lu et al. (2006) and Lu (2004) demonstrated the seasonal differences in the EAP teleconnection between early summer (June) and late summer (August); also, the EAP teleconnection is affected by the mid-latitude teleconnection. Therefore, the wave-flow interaction in the mid-high latitude in Eurasia and the interaction of the meridional and zonal teleconnections may have a joint influence on the climate anomalies over EA, especially in NA. Ogasawara and Kawamura (2007, 2008) defined the mid-high-latitude teleconnection as the West Asia–Japan (WJ) and Europe–Japan (EJ) patterns, and found that the WJ or EJ pattern and PJ teleconnection pattern were inter-configured, with high-frequency and low-frequency components, affecting the EA surface temperature and summer monsoon circulation. The 10–30-day variability of summer precipitation over southeastern China during the period of 1979–2015 (Li and Mao, 2019) and the devastating floods over the Yangtze Basin during 1998 (Li and Mao, 2018) were both affected by

the Rossby wave that propagates to EA at mid-high latitudes in the upper troposphere through the vorticity advection; meanwhile, the EAP region triggers vertical mechanisms to further enhance the strong updraft (downdraft) over the south of the middle and lower reaches of the Yangtze River Valley. Chen et al. (2019) pointed out that the persistent precipitation extremes in the Yangtze River Valley have the most direct relationship with the EAP teleconnection, whereas the EU and SR teleconnection types need to be exerted via their liaison with the EAP teleconnection and thus affecting the persistent precipitation extremes in the Yangtze River Valley. Previous studies focus on the effects of climate caused by a single teleconnection, but few studies concentrate on the synergistic effect of EU and EAP teleconnections on the climate anomalies in NA and on the mechanism analysis of the interaction between these two teleconnections.

In addition, the western and middle parts of NA contain the main livestock bases, and the eastern part of NA contains the main agriculture bases and commercial centers in the Asian region. The climate in NA is also affected by the mid-high-latitude dry cold airflow and warm humid airflow from the low latitude. The EAP teleconnection mainly reflects the changes of the meridional circulation system, whereas the EU teleconnection denotes the eastward propagation of the circulation wave originated from the North Atlantic. The EU zonal wave transported by the Rossby waves can expand from the North Atlantic to EA. The intersection of the EAP and EU teleconnections are mainly overlapped in the NA region. Therefore, it is necessary to study the joint effect of the EAP–EU teleconnection on impacting precipitation in NA, which may be of great help for understanding the flood and drought mechanisms over this region.

Based on the above statement, an in-depth study of EAP–EU co-action will help us to better understand the causes of precipitation anomalies in EA and NA. Therefore, this paper will analyze the relationship between the EAP and EU teleconnections, focus on their co-action on the climate anomalies over NA, and briefly discuss the proper reason from the atmospheric process. The rest of this paper is organized as follows: A description of the study area, the data, and the methodology is presented in Section 2; the main results are addressed in Section 3; and the brief conclusions are given in Section 4.

2. Study area and data

In this study, NA is defined as the region 70°–160°E, 30°–70°N, and the following datasets are used: (1) The Global Precipitation Climatology Project (GPCP) monthly precipitation observation dataset, which is used for validation of the summer (June, July, and August) precipitation from 1979 to 2015; (2) the National Centers for Environmental Prediction and the National Center for Atmospheric Research's monthly reanalysis dataset. The variables used include the surface pressure, meridional winds, zonal winds, and specific humidity on a regular grid with a horizontal resolution of 2.5° × 2.5°.

The EAP index is defined as below (Huang, 2004):

$$I_{\mathrm{EAP}} = -\frac{1}{4}Z^*(20°\mathrm{N}, 125°\mathrm{E}) + \frac{1}{2}Z^*(40°\mathrm{N}, 125°\mathrm{E}) - \frac{1}{4}Z^*(60°\mathrm{N}, 125°\mathrm{E}). \quad (1)$$

According to the studies of Wallace and Gutzler (1981) and Wakabayashi and Kawamura (2004), the EU index is defined as below:

$$I_{\mathrm{EU}} = -\frac{1}{4}Z^*(55°\mathrm{N}, 20°\mathrm{E}) + \frac{1}{2}Z^*(55°\mathrm{N}, 75°\mathrm{E}) - \frac{1}{4}Z^*(52.5°\mathrm{N}, 110°\mathrm{E}). \quad (2)$$

In Eqs. (1) and (2), Z represents the normalized monthly average geopotential height anomaly at 500 hPa.

3. Results

3.1 *Characteristics of summer precipitation patterns under EAP–EU configurations*

According to Eqs. (1) and (2), the normalized indices of EAP and EU during the period of 1948–2015 are presented in Fig.1. It is evident that both EAP and EU teleconnection indices show obvious interannual variations. The EU index also exhibits interdecadal variability as the EU index changes from its most positive phase before the early 1990s to its most negative phase after the early 1990s. The 30-yr smooth correlation between the EAP and EU indices has a rapid decrease around 1980 (Figs. 1b, c). The correlation coefficient between the EAP and EU teleconnection indices is 0.03 for the period of 1979–2015 and 0.35 for 1948–1978, indicating that EAP and EU teleconnection patterns are independent of each other after 1979. That is to say, the relationship between the two teleconnections has an adjustment around 1979. Therefore, it is necessary to study the EAP–EU joint effects on summer precipitation in EA and NA before and after 1979, respectively. This study mainly reveals the configurations of EAP and EU teleconnection anomalies and their corresponding impact on summer precipitation in NA during the period of 1979–2015, which matches well with the period of the

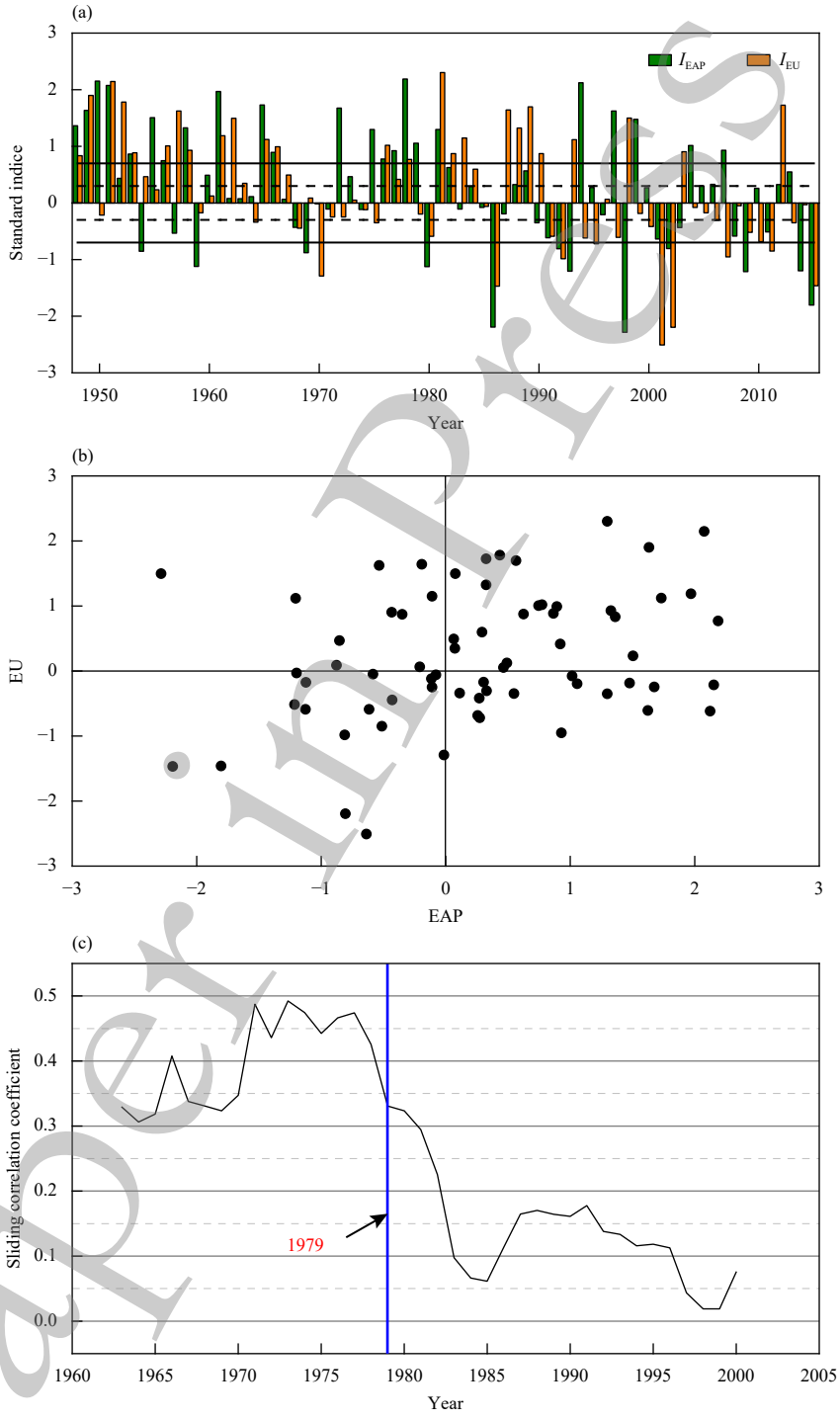

Fig. 1. (a) The time series (the black solid and dashed lines are the 0.7 and 0.3 std deviations respectively), (b) The scatter diagram of EAP and EU standardization indices, and (c) The smooth correlation coefficient between EAP and EU indices with a 30-yr window and 1-yr move step.

GPCP dataset.

For the purpose of further studies, the mutual configuration between EAP and EU teleconnections, the EAP and EU indices are divided into four categories: In Category I (II), EAP and EU index anomalies are in the same phase (the same positive or negative anomalies); and in Category III (IV), EAP and EU index anomalies are in the opposite phase (the EAP index being a positive (negative) phase and the EU index being a negative (positive) phase). In order to better express the differences between the EAP and EU indices in the four categories and to ensure that the number of years is as large

as possible, we have chosen the absolute values of the EAP and EU indices to be larger than 0.3-time standard (std) deviations as the selected criterion. Table 1 illustrates that, when the EAP and EU indices are in the positive phase for six years (Category I), the EAP and EU indices are in the negative phase for nine years (Category II), the EAP index is in the positive phase and the EU index is in the negative phase for six years (Category III), and the EU index is in the positive phase and the EAP index is in the negative phase for three years (Category IV). The EAP and EU indices in the same phase are for 15 years (Categories I and II), and those in the opposite phase are for nine years (Categories III and IV), reflecting that the EAP and EU indices are more likely to occur when they are both active in the same phase. In order to better study the role of EAP and EU teleconnections, the characteristics of precipitation and circulation in the four categories are given below.

Figure 2 gives the composite anomalies of summer precipitation in NA corresponding to different EAP–EU configurations. For Category I, when the EAP and EU indices both present positive phases, the summer precipitation anomaly in NA is mainly distributed as the "– + –" structure from northwest to southeast. Less precipitation is distributed over the Ural Mountain area, coastal East China to Japan, and surrounding sea areas, whereas more precipitation is located in the regions from central China to the east of Baikal Lake and Russian Far East (Fig. 2a). Meanwhile, precipitation anomalies in northern NA (70°–160°E, 50°–70°N) are characterized by an east–west reverse-phase structure and featured by the north–south reverse-phase distribution in eastern NA (120°–160°E, 30°–70°N). For Category II, when both the EAP and EU teleconnections have negative phases (Fig. 2b), precipitation over the EU continent exhibits the opposite spatial abnormal structure to that which is presented in Fig. 2a. Positive anomalies are mainly concentrated in the Ural Mountain area and Japan and its surrounding sea areas, whereas negative anomalies are characterized in central China to Mongolia and eastern Russia. The west–east pattern in northern NA and the north–south pattern in eastern NA are also observed in Fig. 2b.

For Category III, when the EAP index is positive and

Table 1. Years for the four types of EAP–EU configurations corresponding to the 0.3, 0.5, and 0.7 std deviation thresholds during the period of 1979–2015

Type	I_{EAP}	I_{EU}	0.3 std	0.5 std	0.7 std
I	+	+	1981, 1982, 1984, 1988, 1989, 2012	1981, 1989	1981
II	–	–	1980, 1986, 1991, 1992, 2001, 2002, 2009, 2011, 2015	1980, 1986, 1991, 1992, 2001 2002, 2009, 2015	1986, 1992, 2002, 2015
III	+	–	1994, 1995, 1997, 2000, 2007, 2010	1994, 1997, 2007, 2010	2007, 2010
IV	–	+	1993, 1998, 2003	1993, 1998, 2003	1993, 1998, 2003

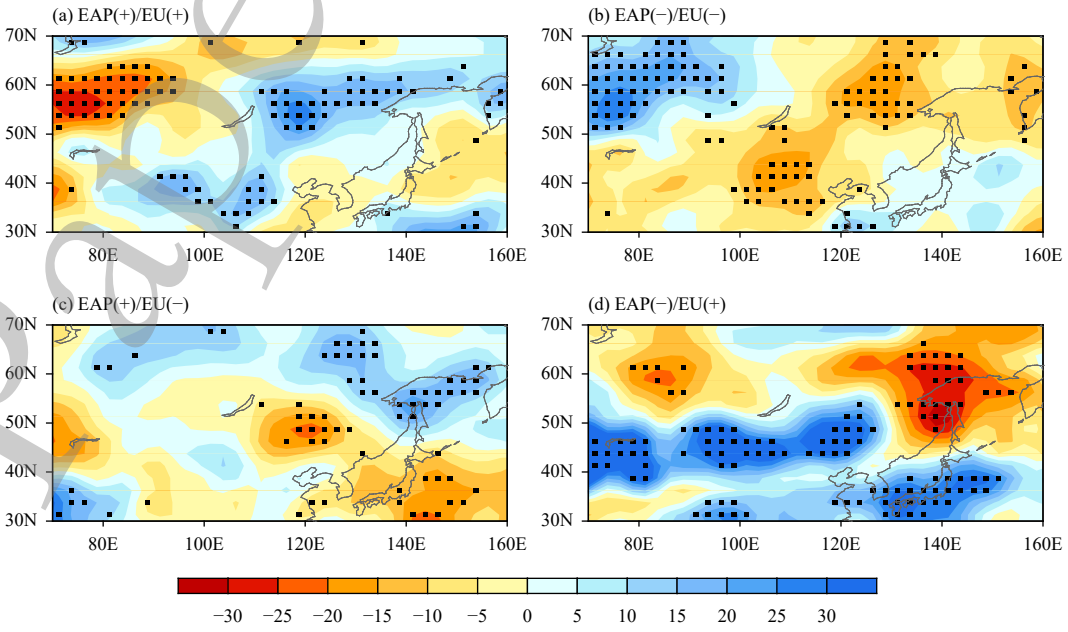

Fig. 2. Spatial distributions of the percentage of summer precipitation anomalies in NA for different EAP–EU configurations (color scale; %). Dotted areas indicate the 90% confidence level. (a) EAP(+)/EU(+), (b) EAP(−)/EU(−), (c) EAP(+)/EU(−), and (d) EAP(−)/EU(+).

the EU index is negative, compared with the spatial distribution of Category I, the NA summer precipitation is mainly characterized by a "+ −" dipole distribution from north to south (Fig. 2c). The west–east pattern of the precipitation anomaly in northern NA changed to a zonal consistent structure, whereas the north–south opposite phase feature was maintained in eastern NA. For Category IV, when the EAP index is negative and the EU index is positive (Fig. 2d), the precipitation anomalies in the northern EU region (70°–160°E, 50°–70°N) are significantly less than normal, whereas the majority of precipitation in the southern part of NA (70°–160°E, 30°–50°N) is more than normal, showing a "− +" dipole pattern in the meridional direction. Summer precipitation patterns corresponding to Categories I and II of the EAP–EU configuration can also be found in the first and second modes of the empirical orthogonal function (EOF) in the summer precipitation over NA (Gong et al., 2017). Therefore, the spatial distributions of NA summer precipitation are obviously different from each other for the two types of EAP–EU configuration, which calls for further study on the EAP–EU co-action through the atmospheric composite analysis.

In order to further confirm the meaning of the EAP–EU configuration corresponding to the NA summer precipitation pattern, the two EOF leading zonal modes are presented in Fig. 3. The notable feature of EOF1 (Fig. 3a) is the north-dry/south-wet pattern, with major positive anomalies located to the northwest of Baikal Lake and Okhotsk Sea, whereas a rainy belt dominates the region between 30°N and 50°N from west to east. The EOF1 has a very similar spatial feature to the summer precipitation anomaly distribution of Category IV of the EAP–EU configuration (Fig. 2d). The spatial pattern EOF2 (Fig. 3b) shows a northwest–southeast wave structure. Two positive lobes are respectively distributed to the west of Baikal Lake and Japan and its offshore area, whereas two negative lobes are respectively located in North China and Russian Far East. The spatial pattern of EOF2 is quite similar to the summer precipitation anomaly distribution of Category II of the EAP–EU configuration (Fig. 2b). Therefore, the EAP–EU configuration corresponded patterns revealed in Fig. 2 reflect the major spatial characteristics of summer precipitation anomalies in NA.

When the EAP and the EU indices are both in positive phases, the composite anomalies of the 500-hPa geopotential height exhibit a "+ − +" tripole wave train from northwest NA to southeast. The Ural Mountain area, Northeast China, and Japan are all controlled by positive anomalies, whereas negative anomalies dominate the Baikal Lake area (Fig. 4a); the coupled anticyclonic and cyclonic anomalies are also observed at both the 850- and 200-hPa wind fields (Fig. 5a), showing that the wavelike pattern has an equivalent barotropic structure in the vertical direction. Meanwhile, the 500-hPa geopotential height field in northern NA shows zonal opposite phase characteristics, and in eastern NA, it shows the meridional opposite phase. According to the omega equation (Chen and Huang, 2012), the anomalies at the 500-hPa geopotential height and wind field may cause the downward motion in the Ural Mountain area, Northeast China, and Japan, as well as the upward motion in the Baikal Lake area, which can lead to the precipitation anomaly structure presented in Fig. 1a. The tripole wavelike pattern is similar to the teleconnection Europe–China (EC) pattern defined by Chen and Huang (2012), which propagates through an arc path (Hoskins and Karoly, 1981). When the EAP and EU teleconnections are both in negative phases, atmospheric circulation statuses at the 200-, 500-, and 850-hPa (Figs. 4b, 5b) fields show the opposite anomalous phase distributions to that of the EAP–EU consistent positive phases (Figs. 4a, 5a).

When the EAP index is positive and the EU index is

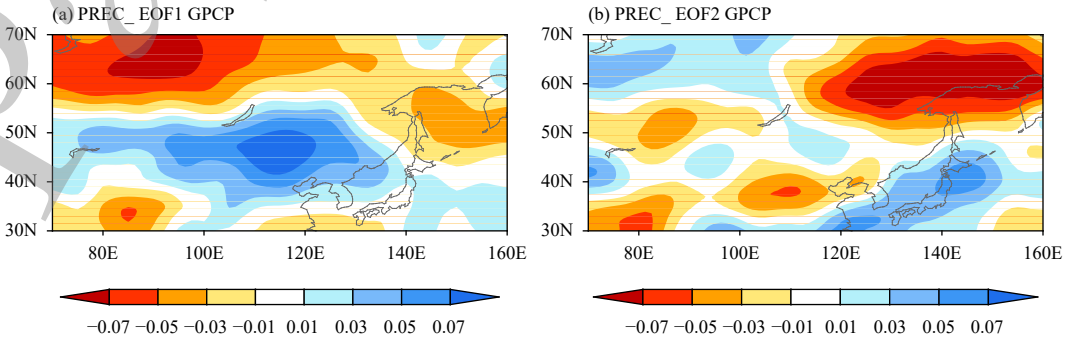

Fig. 3. The spatial pattern of (a) EOF1 and (b) EOF2 for summer precipitation anomalies over the NA region (30°–70°N, 70°–160°E) during the period of 1979–2015 for GPCP. The variance percentage of reanalysis is 15.3% for EOF1 and 12.5% for EOF2, respectively.

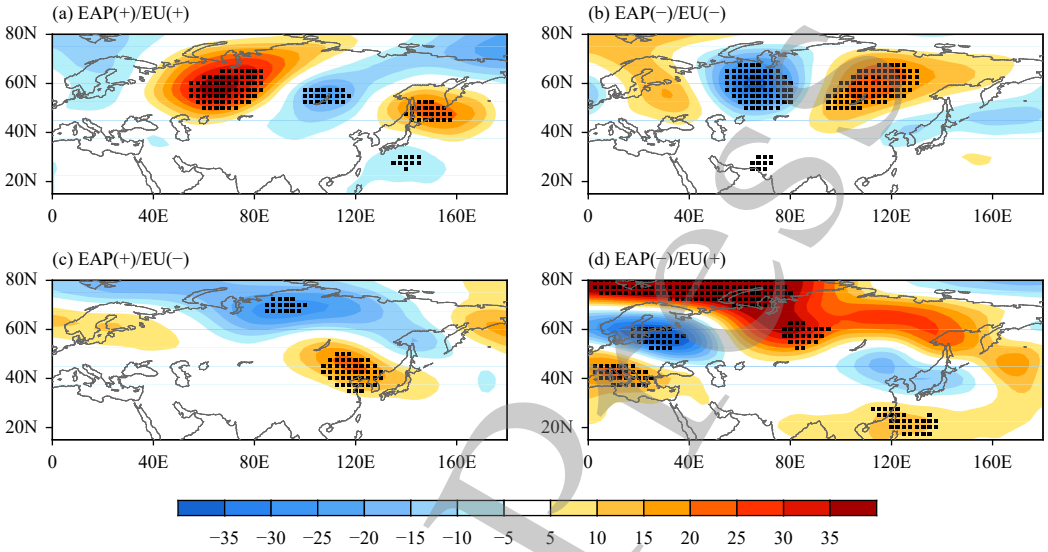

Fig. 4. The spatial distribution pattern of the height field at 500 hPa for EAP and EU indices under the 0.3 std deviation (gpm). The black point region indicates the 95% confidence level. (a) EAP(+)/EU(+), (b) EAP(−)/EU(−), (c) EAP(+)/EU(−), and (d) EAP(−)/EU(+).

negative, the "− +" dipole distribution is observed from north to south at the 500-hPa geopotential height field. Most parts of Russia are controlled by negative anomalies (Fig. 4c) and anticyclonic wind anomalies at both low and high levels (Fig. 5c), whereas the Baikal Lake area to Northeast China and Japan are dominated by positive height anomalies and cyclonic wind anomalies. With this spatial distribution of the atmospheric circulation, it is not surprising to see the dipole pattern of summer precipitation indicated in Fig. 1c. It is also noted that the geopotential height shows the west–east consistent negative anomalies over northern NA and overall north–south reverse-phase characteristic in NA. This might be the direct reason for the precipitation anomaly distribution changes to the zonal consistent phase structure in northern NA and the continuation of the north–south opposite phase pattern in eastern NA. When the EAP index is negative and the EU index is positive, the reverse-phase pattern with the "+ −" dipole distribution in the meridional direction is exhibited in the circulation field from low to high levels with an equivalent barotropic structure (Figs. 4d, 5d).

Additionally, we respectively use the 0.5 and 0.7 std deviations as thresholds for the EAP–EU configuration

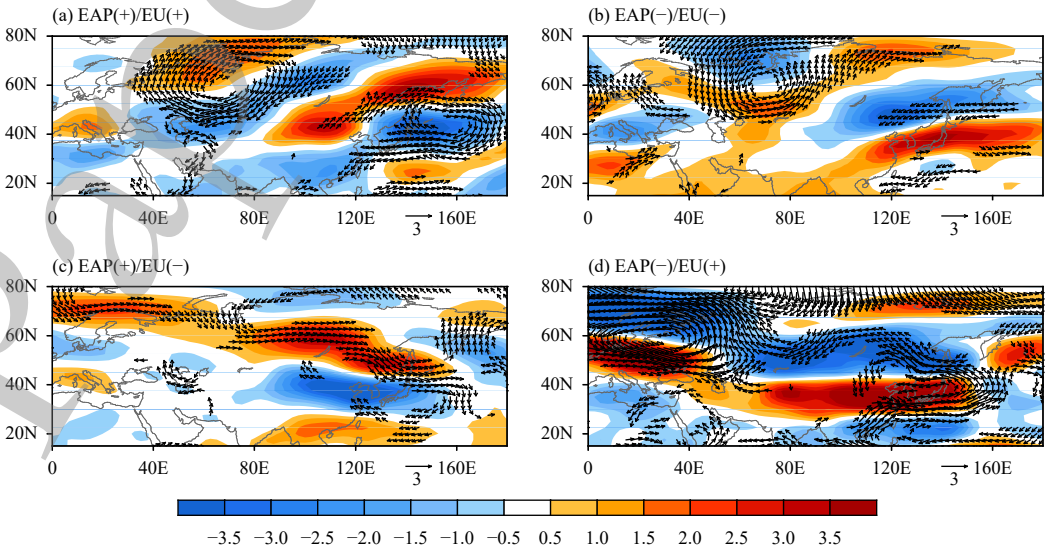

Fig. 5. The spatial distribution of the wind field for EAP and EU indices under different configurations. The shadow part is the 200-hPa wind field (color scale; m s^{-1}), and the vector is an 850-hPa wind field (vectors; m s^{-1}) which shows the only vectors above the 95% confidence level. (a) EAP(+)/EU(+), (b) EAP(−)/EU(−), (c) EAP(+)/EU(−), and (d) EAP(−)/EU(+).

selection during the period of 1979–2015 (Table 1). It is obvious that the number of selected sample years gradually decreases with the increase of thresholds. The spatial distribution patterns of the geopotential height at 500 hPa for the four types of EAP–EU configurations corresponding to the 0.5 (Fig. 6) and 0.7 std deviation (Fig. 7) thresholds are quite similar to that of Fig. 4. Furthermore, we present the geopotential height at 500 hPa for EAP–EU configurations corresponding to the 0.7 std deviation threshold during the period of 1948–2018 (Fig. 8). The geopotential height anomaly distribution shows a similar pattern to that of the 0.3 std deviation during the period of 1979–2018. Therefore, in order to meet the demand of the sample size and to properly present the summer precipitation and circulation characteristics of the EAP–EU configurations, this study mainly uses the 0.3 std deviation as the threshold for EAP–EU configuration selection.

As previously stated, the EU teleconnection is one of five important teleconnection wave trains propagating from west to east over the EU continent. Normally, it presents high correlation centers located at (55°N, 20°E), (55°N, 75°E), and (55°N, 110°E). However, because of the influence of the meridional pattern over the EA and West Pacific, i.e., the EAP/PJ teleconnection, the spatial pattern of the EU teleconnection in the region of NA (overlapped with the northern lobe of the EAP teleconnection) may change some years, although its upper

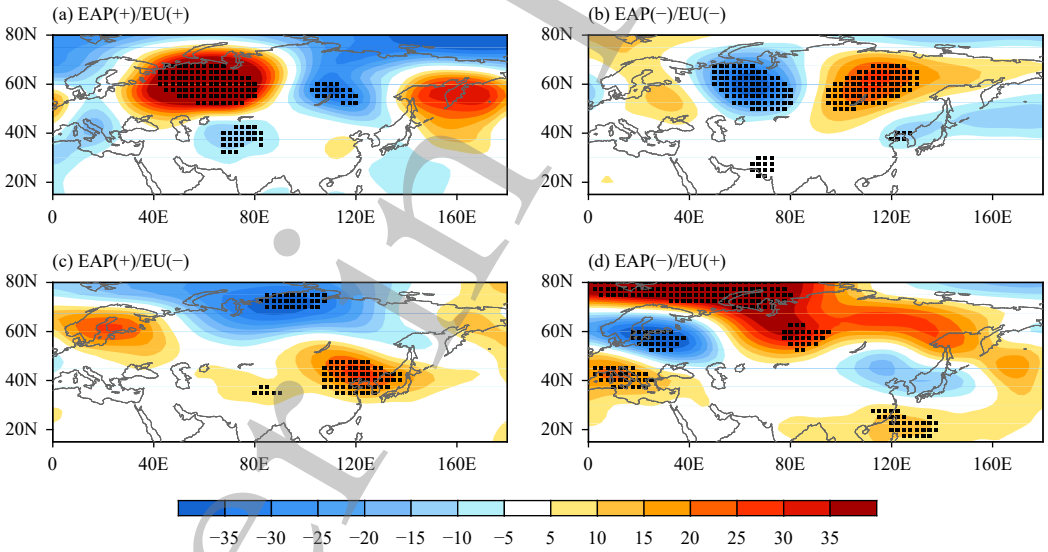

Fig. 6. As in Fig. 4 but for the 0.5 std deviation.

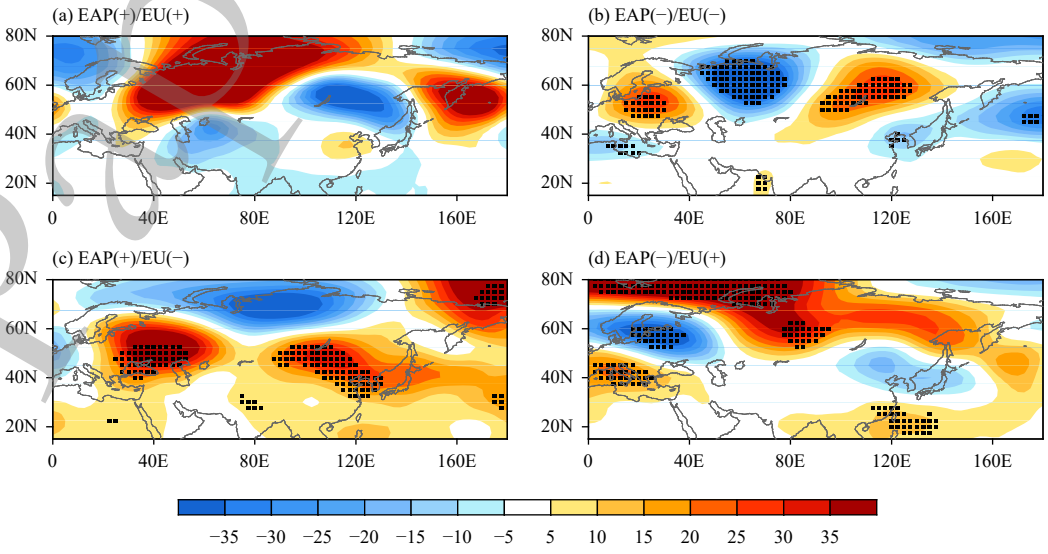

Fig. 7. As in Fig. 4 but for the 0.7 std deviation.

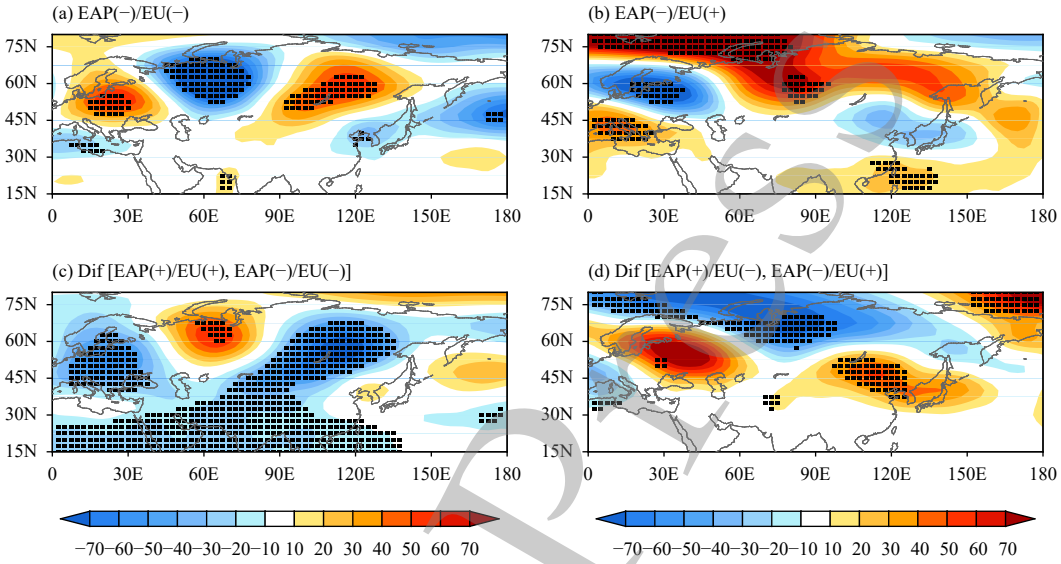

Fig. 8. The spatial distribution pattern of the geopotential height field at 500 hPa for EAP and EU indices under the 0.7 std deviation (gpm). (a) EAP(−)/EU(−), (b) EAP(−)/EU(+), (c) EAP(+)/EU(+) minus EAP(−)/EU(−), and (d) EAP(+)/EU(−) minus EAP(−)/EU(+).

reaches keep the obvious teleconnection structure. This study revealed the circulation patterns under four types of the EAP–EU configuration (Fig. 4). It was found that, when the EAP and EU teleconnections existed in the same phase, Category I (II), the zonal triple structure maintains a geopotential height at 500 hPa from eastern Europe to the Sea of Japan. Although the EAP and EU teleconnections are out of phase, Category III (IV), the teleconnection is not a well-structured one dictated by one or two very strong centers, as exemplified by Figs. 4c, d. The reason might be that the northern negative (positive) lobe of the EAP teleconnection overlaps with the central negative (positive) lobe and the eastern positive (negative) lobe of the EU teleconnection; this may strengthen the negative (positive) anomalies over the Baikal Lake region and weaken the positive (negative) anomalies over the Haiti Okhotsk region, leading to consistent negative (positive) anomalies distributed from central China to Baikal Lake and Russian Far East. Therefore, as summarized in Fig. 11, the Category I (II) configuration represents the significant differences between the east and west part of northern NA, whereas the Category III (IV) configuration implies the consistent anomalies in northern NA. Furthermore, the south–north opposite pattern in eastern NA is maintained in both the categories.

Therefore, the EAP and EU teleconnections, NA summer precipitation, and mid-high-latitude circulations are closely linked to each other. For the Category I configuration, the summer precipitation and circulation in NA from northwest to southeast present a tripole wave pattern; whereas for the Category II configuration, the precipitation and circulation anomaly fields show a dipole feature in the meridional direction. Meanwhile, the Category I (II) configuration represents the significant differences between the east and west parts of northern NA, whereas the Category III (IV) configuration implies consistent anomalies in northern NA. Furthermore, the south–north opposite pattern in eastern NA is maintained in both the categories.

3.2 *The synergistic impact of EAP and EU teleconnections*

The EAP teleconnection pattern mainly presents the distribution of the meridional tripole structure, reflecting the effects of low latitude circulations on precipitation in EA (Huang, 2004; Zhou T. J. et al., 2009). The EU teleconnection shows the zonal wave pattern distribution, which reflects the effect of mid-high-latitude circulation on precipitation across the EU continent (Kosaka et al., 2009; Chen and Huang, 2012). In this section, we analyze the individual impact of the EAP and EU teleconnections on the summer precipitation in the mid-latitudes of Eurasia and propose the synergistic effect of the two categories on the EAP–EU configuration.

The spatial distributions of the 500-hPa height field and precipitation field regressed onto the EAP and EU indices are shown in Figs. 9, 10, respectively. When the EAP index is positive, in the 500-hPa height field, the region from Baikal Lake to Okhotsk Sea is dominated by negative anomalies, and North China and Japan are controlled by positive anomalies (Fig. 9a), resulting in an anomalous increase in precipitation in the region from Baikal Lake to Okhotsk Sea and an anomalous decrease

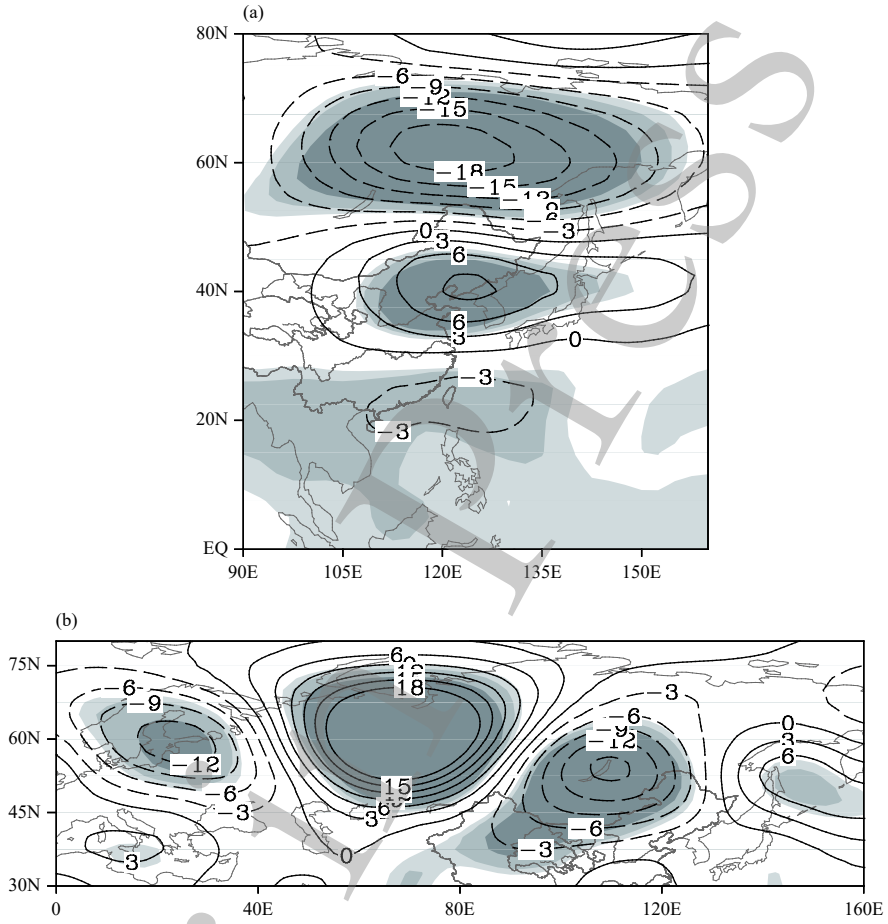

Fig. 9. The spatial distribution of the 500-hPa height field regressed by the (a) EAP and (b) EU indexes. Shadings denote the 90%, 95%, and 99% confidence levels, respectively.

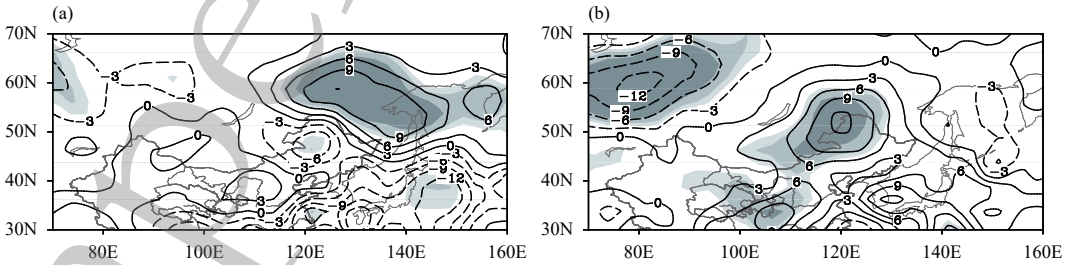

Fig. 10. As in Fig. 9 but for the precipitation regressed onto the (a) EAP and (b) EU indexes.

in precipitation in the region from Northeast China to Japan (Fig. 10a). The EAP teleconnection mainly affects summer precipitation in eastern NA (120°–160°E, 30°–70°N) and creates north–south opposite meridional features (Huang J. P. et al., 1993; Huang R. H. et al., 2012). When the EU index is in a positive phase, the 500-hPa geopotential height in the mid-latitude EU region is characterized by a "+ − +" wavelike pattern from the northwest to the southeast, and the anomaly centers are mainly located in Ural Mountain, Baikal Lake, and Okhotsk Sea areas (Fig. 9b), leading to more precipitation in Ural Mountain and Okhotsk Sea areas as well as less precipitation over Baikal Lake (Fig. 10b). Thus, the EU type mainly affects the zonal mode of the summer precipitation in NA, especially in the northern region. Therefore, the EAP teleconnection mainly leads to a north–south dipole distribution in eastern NA, whereas the EU teleconnection mainly affects the zonal differences of summer precipitation in northern NA (Huang, 2004; Chen and Huang, 2012).

Figure 11 shows schematic diagrams explaining the EAP–EU configuration in the 500-hPa geopotential

height field. It can be seen from Fig. 11a that the EU index is positive with an abnormally high system located over the Ural Mountain and Okhotsk Sea areas, with an abnormally low system distributed over the Baikal Lake region. The EAP index is positive from Baikal Lake to Haiti Okhotsk, which is controlled by a low-pressure system, whereas the area from Northeast China to Japan is dominated by a high-pressure system. The northern negative lobe of the EAP teleconnection overlaps with the central negative lobe and eastern positive lobe of the EU teleconnection, which may strengthen the negative anomalies over the Baikal Lake region and weaken the positive anomalies over the Haiti Okhotsk region, leading to consistent negative anomalies distributed from central China to Baikal Lake and Russian Far East. It is also because the EU western positive lobe and EAP southern positive lobe maintain their original phases, with the 500-hPa height presenting the zonal arc tripole pattern (Fig. 2a), and northern NA mainly shows the west–east reverse-phase structure. In eastern NA, because of the dominant role played by the EAP teleconnection, the geopotential height maintains the dipole structure from north to south. According to the omega equation, the spatial distribution of the geopotential height anomalies will motivate the summer precipitation anomaly pattern presented in Fig. 1a. According to the circulation anomalies, the precipitation over NA mainly presents the "+ − +" pattern from eastern Europe to the Sea of Japan. This precipitation structure is quite consistent with that of Fig. 2b. The same mechanism can explain the possible co-action of the configuration with both EAP and EU being in negative phases (figure omitted).

When the EAP is positive and the EU is negative (Fig. 11b), the negative lobe of the EAP teleconnection over the area from Baikal Lake to Okhotsk Sea can weaken the positive anomalies of Eurasia over the Baikal Lake region and form a negative anomaly band in northern NA. Additionally, the positive anomalies of Eurasia over the Baikal Lake region are also somewhat overlapped with the positive lobe of the EAP pattern, which may strengthen the positive anomalies in these regions. Accordingly, the spatial distribution of the geopotential height at the 500-hPa field presents a north-negative south-positive pattern, causing more precipitation in northern NA but less in southern NA (Fig. 1b). Corresponding to the circulation anomalies, precipitation from

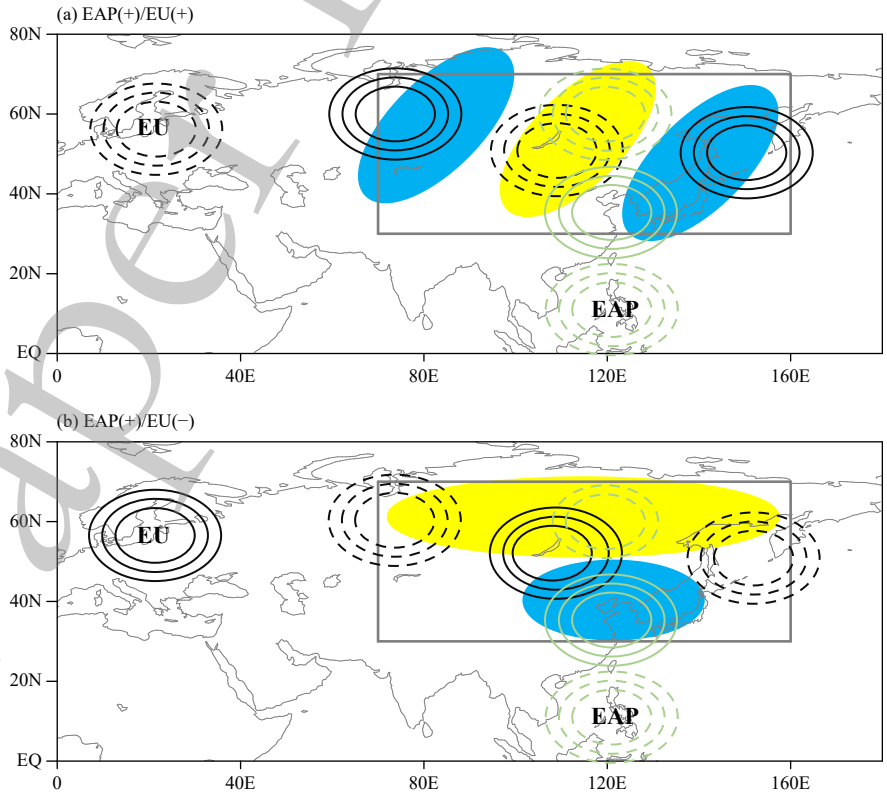

Fig. 11. Interaction diagrams of EAP and EU teleconnections under different configurations. (a) EAP(+)/EU(+) and (b) EAP(+)/EU(−). The rectangular box represents the North Asian region. Black and green lines represent EU and EAP teleconnections, respectively, whereas the solid and dashed contours indicate the positive and negative anomalies, respectively. The light-blue and the light-yellow ellipses represent more and less precipitation in NA, respectively.

eastern Europe to Russian Far East is mainly dominated by negative values, whereas the area from North China to the Sea of Japan may have more precipitation. This precipitation structure is quite consistent with that of Fig. 2d. The same mechanism can be used to explain the possible co-impact of the configuration with negative EAP and positive EU (figure omitted).

3.3 *The linear simulation of EAP–EU co-action*

In order to verify the above analysis, based on the EAP index (I_{EAP}) and EU index (I_{EU}), a simplified two-element linear regression model was constructed to simulate the co-action of the EAP–EU configuration on the 500-hPa height and summer precipitation in NA.

$$P = aI_{EAP} + bI_{EU} + e_P, \quad (3)$$

$$H = cI_{EAP} + dI_{EU} + e_H, \quad (4)$$

where P is the summer precipitation; H is the 500-hPa height; coefficients a, b, c, and d are determined by the binary regression method; and e is the residual term.

The EAP and EU indices are put into Eqs. (3) and (4), respectively, and the linear model can produce the regressed new precipitation and geopotential height fields. When only considering the case where the EAP and EU indices are in the positive phase, and the EAP and EU are in the positive and negative phases respectively, the composite plots of the new 500-hPa geopotential height and precipitation field are given in Figs. 12, 13, respectively. For the Category I EAP–EU configuration, when the EAP and EU indices are both positive, the 500-hPa geopotential height mainly presents the "+ − +" tripole distribution from northwest to southeast (Fig. 12a), with the anomalous positive centers distributed in Ural Mountain and Okhotsk Sea areas; the negative center is located in the eastern Baikal Lake area, which is consistent with the observed spatial pattern (Fig. 4a). This spatial consistency is also exhibited in the regressed (Fig. 13a) and observed (Fig. 2a) summer precipitation fields. For Category II, when the EAP index is positive and EU index is negative, the regressed 500-hPa height field in NA presents the "+ −" dipole structure in the meridional direction (Fig. 12b), with a positive anomaly belt distributed from the Ural Mountain area to Baikal Lake and Okhotsk Sea and negative anomalies concentrated in North China to Japan and the maritime region, which is similar to the observed spatial anomaly distribution (Fig. 4b). The spatial distribution of regressed precipitation is also observed in Fig. 2b. Therefore, the EAP–EU co-action can be reproduced by the regression simulation. Since the other two configurations are similar to the preceding two, respectively, the relevant analysis is not repeated in this study.

In order to further confirm the role that the EAP and EU teleconnections have on influencing the geopotential height and precipitation in NA, the EAP and EU indices are doubled and put into the linear Eqs. (3) and (4), respectively, to obtain new height and precipitation fields. Figures 12c, d; 13c, d show a regressed 500-hPa geopotential height and precipitation on the two-time EAP index and one-time EU index. For the Category I configuration with positive EAP and positive EU (Figs. 12c, 13c), the anomalous anomalies of the geopotential height and

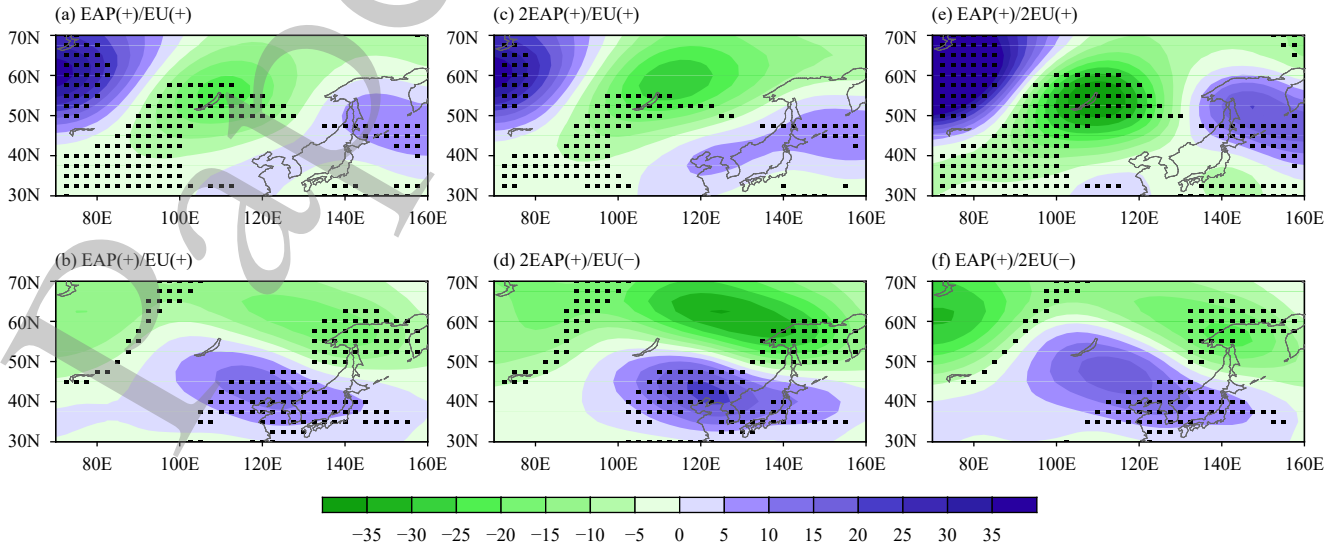

Fig. 12. The binary regression of the summer 500-hPa geopotential height anomalies to EAP and EU indices. (a) EAP(+)/EU(+), (b) EAP(+)/EU(−), (c) 2EAP(+)/EU(+), (d) 2EAP(+)/EU(−), (e) EAP(+)/2EU(+), and (f) EAP(+)/2EU(−). Dotted areas indicate the 90% confidence level.

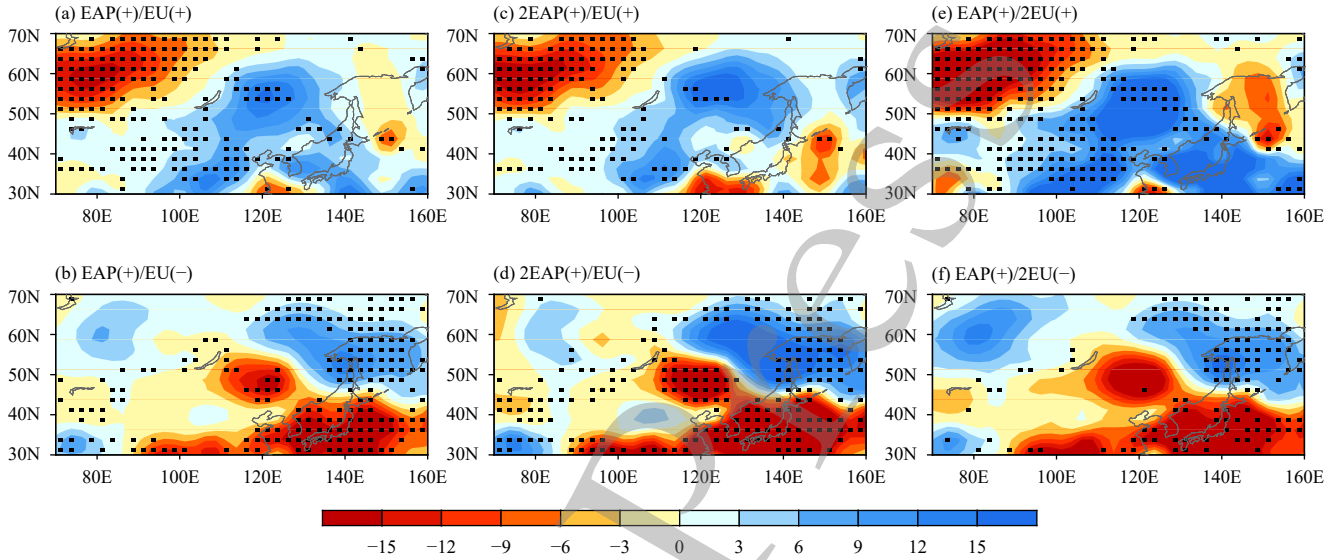

Fig. 13. As in Fig. 12 but for the summer precipitation to EAP and EU indices.

precipitation over the Baikal Lake area to Russian Far East are enhanced because of the enhancement of the EAP effect. The west–east reverse-phase characteristics over northern NA and the feature of the north–south opposite phases over eastern NA are further enhanced. For the Category II configuration with positive EAP and negative EU (Figs. 12d, 13d), the north–south pattern in the meridional direction is obviously enhanced, especially over the eastern NA region. Accordingly, the EAP teleconnection plays a decisive role in strengthening the west–east differences over northern NA for the Category I configuration and enhances the north–south differences over eastern NA for the Category II configuration.

Figures 12e, f; 13e, f show a regressed 500-hPa geopotential height and precipitation on the one-time EAP index and two-time EU index, respectively. For the Category I configuration with positive EAP and positive EU, the zonal wavelike structure in both 500-hPa height (Fig. 12e) and precipitation (Fig. 13e) has been obviously enhanced, indicating that strong EU plays the dominant role in causing the zonal tripole pattern through an arc path across the EU continent. The enhanced EU effect also replaces the west–east reverse-phase distribution by three anomalous centers. This regressed three-center wave train associated with the EC teleconnection (Chen and Huang, 2012) is the result of propagation of the stationary Rossby wave activity with the source region over the North Atlantic. The only difference is that the eastern anomalous center of the EC teleconnection is moved somewhat southward. For the Category II configuration with positive EAP and negative EU, the 500-hPa height anomalies mainly maintain the north-negative south-positive distribution. Compared with the distribution of original EAP and EU regressions, doubling the effect of Eurasia will increase the anomalous significance of meridional differences by enlarging the geopotential height (Fig. 12f) and precipitation (Fig. 13f) anomalies over the Ural Mountain area. Accordingly, the EU teleconnection adjusts the anomalous phase distribution in NA, especially influencing the anomaly distribution over northern NA.

Since the first two leading EOF modes somehow represent the summer precipitation patterns of the EAP–EU configuration (Fig. 3), the principal components (PC1 and PC2) may also partially indicate the main annual variability (Fig. 14). The I_{EAP} and I_{EU} regressed principal components ($P1$ and $P2$) according to Eq. (3) are presented in Fig. 14. The correlation coefficients between PC1 and $P1$ and between PC2 and $P2$ are respectively 0.51 and 0.68, both passing the 95% confidence level. That is to say, the EAP–EU joint effect can reproduce the annual variability of the EAP–EU configuration defined by the NA summer precipitation pattern.

$$P1 = 0.414 \times I_{EAP} + 4.578 \times I_{EU} - 0.00025, \quad (5)$$

$$P2 = -4.741 \times I_{EAP} + 3.980 \times I_{EU} - 0.00021. \quad (6)$$

Based on the above analysis, the mechanism of the synergistic impact of the EAP and EU teleconnections on climate anomalies in NA presumed in Section 3.2 is verified through the linear model simulation. The EAP northern lobe, when overlapped with the EU central and eastern lobes, can adjust the geopotential anomalies over the region from Baikal Lake to Russian Far East, causing the EAP–EU co-action on summer precipitation in NA. The EAP–EU co-action can motivate the zonal tripole wave-

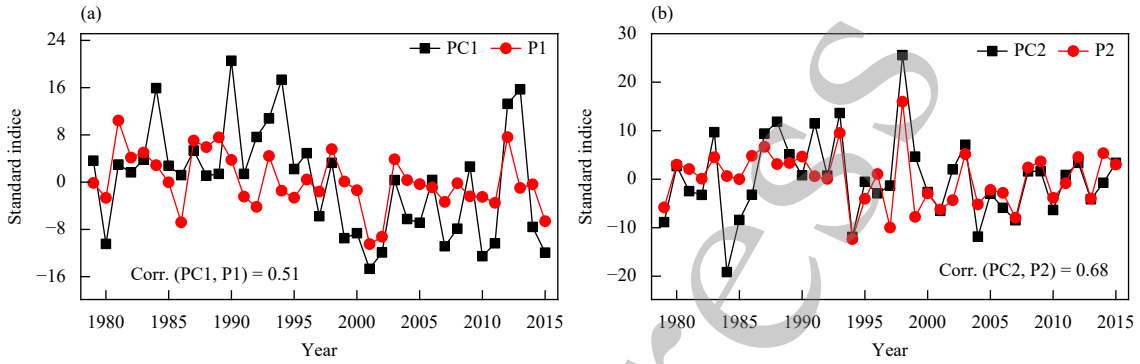

Fig. 14. Principal components (PCs) of (a) EOF1 and (b) EOF2 corresponding to Figs. 3a, 3b.

like pattern in the geopotential height and precipitation field if the EAP and EU teleconnections have the same anomalous phase; it can also trigger the meridional dipole structure on the condition that the EAP and EU teleconnections are in opposite anomalous phases.

4. Brief conclusions

Since both EAP and EU teleconnections have great impacts on the climate in EA and NA, this paper mainly analyzed the co-action of EAP–EU configuration on influencing summer climate anomalies in NA. A possible mechanism was proposed to explain the synergistic effects of the EAP–EU configuration by analyzing the individual teleconnection function. Meanwhile, a linear model simulation was also designed for the co-action mechanism. Main conclusions are summarized as follows:

(1) The EAP and EU teleconnection patterns represent meridional circulation and zonal atmospheric circulation anomalies, respectively. The correlation coefficient between EAP and EU is 0.03, indicating that they have an independent relationship with each other and reflecting that the two teleconnections have different effects on summer precipitation in NA. The EAP teleconnection is negatively correlated with precipitation over the extratropical region from middle East China to Japan but positively associated with precipitation in Russian Far East and Okhotsk Sea regions, causing a north–south dipole distribution of precipitation anomalies in eastern NA. The EU teleconnection is negatively correlated with summer precipitation in the Ural Mountain and Okhotsk Sea regions but positively associated with precipitation in the Baikal Lake region, which may lead to the tripole anomalous wavelike structure over northern NA.

(2) The EAP and EU teleconnections have synergistic effects on precipitation in NA. According to the index anomalous phases, the EAP and EU teleconnections can be divided into two categories of configurations: Category I (II) with EAP and EU teleconnections in the same anomalous phase and Category III (IV) with two teleconnections in opposite anomalous phases. The Category I (II) configurations cause precipitation in the Ural Mountain area and Okhotsk Sea, the region from Northeast China to Japan being less (more), and Baikal Lake to Okhotsk Sea being more (less), which leads to summer precipitation in NA mainly presenting the "− + −" ("+ − +") tripole wavelike structure. Category I (II) configurations also show the west–east reverse anomalies of summer precipitation in northern NA and the north–south opposite anomalies in eastern NA. The Category III (IV) configurations reflect that summer precipitation has a consistent anomaly phase in northern NA, whereas precipitation in the eastern region is still characterized by a meridional opposite phase structure, which shows the overall meridional dipole anomalous distribution in NA.

(3) Using the composite analysis and linear model simulation to verify the EAP–EU co-action mechanism that, with the EAP northern lobe overlapped with the EU central and eastern lobes, can adjust the geopotential anomalies over Baikal Lake to Russian Far East, which in turn cause the EAP–EU co-action on summer precipitation in NA. The EAP–EU co-action motivates the zonal tripole wavelike pattern in the geopotential height and precipitation field if the EAP and EU teleconnections have the same anomalous phase; also, it triggers the meridional dipole structure if the EAP and EU teleconnections are in opposite anomalous phases.

The EAP teleconnection pattern, originating from the low latitude circulation system, mainly reflects the influence on the summer climate in EA (Huang and Li, 1987; Nitta, 1987), whereas the EU teleconnection pattern mainly denotes the relationship between the atmospheric anomalies and EA climate over the middle- and high-latitude region (Wallace and Gutzler, 1981; Wen et al., 2009). Although the EU teleconnection's strongest impact mainly presents in winter, the EU teleconnection

pattern also has a significant impact on the summer climate in EA (Lee et al., 2005; Liu et al., 2014). Therefore, both EAP and EU teleconnections have important implications for summer precipitation in NA. This paper mainly determined that the different configurations of EAP and EU teleconnections have impacts on the spatial pattern of summer precipitation in NA, which can also be reflected by the principle modes of summer precipitation in NA. Additionally, the North Atlantic SST can stimulate the EU teleconnection wave train across the EU continent, and the North Pacific SST may affect the EAP teleconnection wave train through local sea–air interactions (Gong et al., 2018b). Accordingly, the North Atlantic SST and North Pacific SST are major external forcing factors affecting summer precipitation in NA. Therefore, it is necessary to conduct in-depth research on the impact of external forcing on EAP and EU teleconnections and especially to reveal EAP–EU configurations relevant to the SST anomalies of the North Atlantic and North Pacific as well as explore the dynamical mechanism. Meanwhile, the quasi-resonant amplification (QRA) is a mechanism that affects extreme summer events in the Northern Hemisphere. Therefore, we also need to pay attention to whether EAP and EU teleconnection patterns will have a QRA phenomenon and impact on summer precipitation in EA (Kornhuber et al., 2017; Mann et al., 2018).

REFERENCES

Barnston, A. G., and R. E. Livezey, 1987: Classification, seasonality and persistence of low-frequency atmospheric circulation patterns. *Mon. Wea. Rev.*, **115**, 1083–1126, doi: 10.1175/1520-0493(1987)115<1083:CSAPOL>2.0.CO;2.

Bjerknes, J., 1969: Atmospheric teleconnections from the equatorial pacific. *Mon. Wea. Rev.*, **97**, 163–172, doi: 10.1175/1520-0493(1969)097<0163:ATFTEP>2.3.CO;2.

Bueh, C., N. Shi, L. R. Ji, et al., 2008: Features of the EAP events on the medium-range evolution process and the mid- and high-latitude Rossby wave activities during the Meiyu period. *Chinese Sci. Bull.*, **53**, 610–623, doi: 10.1007/s11434-008-0005-2.

Chen, G. S., and G. H. Huang, 2012: Excitation mechanisms of the teleconnection patterns affecting the July precipitation in Northwest China. *J. Climate*, **25**, 7834–7851, doi: 10.1175/jcli-d-11-00684.1.

Chen, Y., and P. M. Zhai, 2015: Synoptic-scale precursors of the East Asia/Pacific teleconnection pattern responsible for persistent extreme precipitation in the Yangtze River Valley. *Quart. J. Roy. Meteor. Soc.*, **141**, 1389–1403, doi: 10.1002/qj.2448.

Chen, Y., P. M. Zhai, Z. Liao, et al., 2019: Persistent precipitation extremes in the Yangtze River Valley prolonged by opportune configuration among atmospheric teleconnections. *Quart. J. Roy. Meteor. Soc.*, **145**, 2603–2626, doi: 10.1002/qj.3581.

Dogar, M. M., F. Kucharski, and S. Azharuddin, 2017: Study of the global and regional climatic impacts of ENSO magnitude using SPEEDY AGCM. *J. Earth Syst. Sci.*, **126**, 30, doi: 10.1007/s12040-017-0804-4.

Fan, K., and H. J. Wang, 2004: Antarctic oscillation and the dust weather frequency in North China. *Geophys. Res. Lett.*, **31**, L10201, doi: 10.1029/2004gl019465.

Gong, Z. Q., M. M. A. Dogar, S. B. Qiao, et al., 2017: Limitations of BCC_CSM's ability to predict summer precipitation over East Asia and the Northwestern Pacific. *Atmos. Res.*, **193**, 184–191, doi: 10.1016/j.atmosres.2017.04.016.

Gong, Z. Q., M. M. Dogar, S. B. Qiao, et al., 2018a: Assessment and correction of BCC_CSM's performance in capturing leading modes of summer precipitation over North Asia. *Int. J. Climatol*, **38**, 2201–2214, doi: 10.1002/joc.5327.

Gong, Z. Q., G. L. Feng, M. M. Dogar, et al., 2018b: The possible physical mechanism for the EAP-SR co-action. *Climate Dyn.*, **51**, 1499–1516, doi: 10.1007/s00382-017-3967-4.

Grotjahn, R., R. Black, R. Leung, et al., 2016: North American extreme temperature events and related large scale meteorological patterns: A review of statistical methods, dynamics, modeling, and trends. *Climate Dyn.*, **46**, 1151–1184, doi: 10.1007/s00382-015-2638-6.

Hingmire, D., R. K. Vellore, R. Krishnan, et al., 2019: Widespread fog over the Indo-Gangetic Plains and possible links to boreal winter teleconnections. *Climate Dyn.*, **52**, 5477–5506, doi: 10.1007/s00382-018-4458-y.

Hoskins, B. J., and D. J. Karoly, 1981: The steady linear response of a spherical atmosphere to thermal and orographic forcing. *J. Atmos. Sci.*, **38**, 1179–1196, doi: 10.1175/1520-0469(1981)038<1179:TSLROA>2.0.CO;2.

Huang, G., 2004: An index measuring the interannual variation of the East Asian summer monsoon—The EAP index. *Adv. Atmos. Sci.*, **21**, 41–52, doi: 10.1007/bf02915679.

Huang, J. P., Y. H. Yi, S. W. Wang, et al., 1993: An analogue-dynamical long-range numerical weather prediction system incorporating historical evolution. *Quart. J. Roy. Meteor. Soc.*, **119**, 547–565, doi: 10.1002/qj.49711951111.

Huang, R. H., and W. J. Li, 1987: Influence of the heat source anomaly over the tropical western Pacific on the subtropical high over East Asia. *Proceedings of 1987 International Conference on the General Circulation of East Asia*, Chengdu, 40-51.

Huang, R. H., and F. Y. Sun, 1992: Impacts of the tropical western Pacific on the East Asian summer monsoon. *J. Meteor. Soc. Japan*, **70**, 243–256, doi: 10.2151/jmsj1965.70.1B_243.

Huang, R. H., J. L. Chen, and G. Huang, 2007: Characteristics and variations of the East Asian monsoon system and its impacts on climate disasters in China. *Adv. Atmos. Sci.*, **24**, 993–1023, doi: 10.1007/s00376-007-0993-x.

Huang, R. H., J. L. Chen, L. Wang, et al., 2012: Characteristics, processes, and causes of the spatio-temporal variabilities of the East Asian monsoon system. *Adv. Atmos. Sci.*, **29**, 910–942, doi: 10.1007/s00376-013-0001-6.

Kornhuber, K., V. Petoukhov, S. Petri, et al., 2017: Evidence for wave resonance as a key mechanism for generating high-amplitude quasi-stationary waves in boreal summer. *Climate Dyn.*, **49**, 1961–1979, doi: 10.1007/s00382-016-3399-6.

Kosaka, Y., H. Nakamura, M. Watanabe, et al., 2009: Analysis on the dynamics of a wave-like teleconnection pattern along the

summertime Asian jet based on a reanalysis dataset and climate model simulations. *J. Meteor. Soc. Japan*, **87**, 561–580, doi: 10.2151/jmsj.87.561.

Lee, E. J., J. G. Jhun, and C. K. Park, 2005: Remote connection of the northeast Asian summer rainfall variation revealed by a newly defined monsoon index. *J. Climate*, **18**, 4381–4393, doi: 10.1175/JCLI3545.1.

Li, J. Y., and J. Y. Mao, 2018: The impact of interactions between tropical and midlatitude intraseasonal oscillations around the Tibetan Plateau on the 1998 Yangtze floods. *Quart. J. Roy. Meteor. Soc.*, **144**, 1123–1139, doi: 10.1002/qj.3279.

Li, J. Y., and J. Y. Mao, 2019: Coordinated influences of the tropical and extratropical intraseasonal oscillations on the 10–30-day variability of the summer rainfall over southeastern China. *Climate Dyn.*, **53**, 137–153, doi: 10.1007/s00382-018-4574-8.

Li, J., R. C. Yu, and T. J. Zhou, 2008: Teleconnection between NAO and climate downstream of the Tibetan Plateau. *J. Climate*, **21**, 4680–4690, doi: 10.1175/2008JCLI2053.1.

Li, L., P. M. Zhai, Y. Chen, et al., 2016: Low-frequency oscillations of the East Asia–Pacific teleconnection pattern and their impacts on persistent heavy precipitation in the Yangtze–Huai River Valley. *J. Meteor. Res.*, **30**, 459–471, doi: 10.1007/s13351-016-6024-z.

Lin, Z. D., and R. Y. Lu, 2016: Impact of summer rainfall over southern-central Europe on circumglobal teleconnection. *Atmos. Sci. Lett.*, **17**, 258–262, doi: 10.1002/asl.652.

Liu, Y. Y., L. Wang, W. Zhou, et al., 2014: Three Eurasian teleconnection patterns: Spatial structures, temporal variability, and associated winter climate anomalies. *Climate Dyn.*, **42**, 2817–2839, doi: 10.1007/s00382-014-2163-z.

Lu, R. Y., 2004: Associations among the components of the East Asian summer monsoon system in the meridional direction. *J. Meteor. Soc. Japan*, **82**, 155–165, doi: 10.2151/jmsj.82.155.

Lu, R. Y., Y. Li, and B. W. Dong, 2006: External and internal summer atmospheric variability in the western North Pacific and East Asia. *J. Meteor. Soc. Japan*, **84**, 447–462, doi: 10.2151/jmsj.84.447.

Mann, M. E., S. Rahmstorf, K. Kornhuber, et al., 2018: Projected changes in persistent extreme summer weather events: The role of quasi-resonant amplification. *Sci. Adv.*, **4**, eaat3272, doi: 10.1126/sciadv.aat3272.

Nitta, T., 1987: Convective activities in the tropical western Pacific and their impact on the Northern Hemisphere summer circulation. *J. Meteor. Soc. Japan*, **65**, 373–390, doi: 10.2151/jmsj1965.65.3_373.

Nitta, T., and Z. Z. Hu, 1996: Summer climate variability in China and its association with 500 hPa height and tropical convection. *J. Meteor. Soc. Japan*, **74**, 425–445, doi: 10.2151/jmsj1965.74.4_425.

Ogasawara, T., and R. Kawamura, 2007: Combined effects of teleconnection patterns on anomalous summer weather in Japan. *J. Meteor. Soc. Japan*, **85**, 11–24, doi: 10.2151/jmsj.85.11.

Ogasawara, T., and R. Kawamura, 2008: Effects of combined teleconnection patterns on the East Asian summer monsoon circulation: Remote forcing from low- and high-latitude regions. *J. Meteor. Soc. Japan*, **86**, 491–504, doi: 10.2151/jmsj.86.491.

Srinivas, G., J. S. Chowdary, Y. Kosaka, et al., 2018: Influence of the Pacific–Japan pattern on Indian summer monsoon rainfall. *J. Climate*, **31**, 3943–3958, doi: 10.1175/JCLI-D-17-0408.1.

Tachibana, Y., T. Nakamura, and N. Tazou, 2007: Interannual variation in snow-accumulation events in Tokyo and its relationship to the Eurasian pattern. *SOLA*, **3**, 129–132, doi: 10.2151/sola.2007-033.

Takaya, K., and H. Nakamura, 2013: Interannual variability of the East Asian winter monsoon and related modulations of the planetary waves. *J. Climate*, **26**, 9445–9461, doi: 10.1175/JCLI-D-12-00842.1.

Ueda, H., T. Yasunari, and R. Kawamura, 1995: Abrupt seasonal change of large-scale convective activity over the western Pacific in the northern summer. *J. Meteor. Soc. Japan*, **73**, 795–809, doi: 10.2151/jmsj1965.73.4_795.

Wakabayashi, S., and R. Kawamura, 2004: Extraction of major teleconnection patterns possibly associated with the anomalous summer climate in Japan. *J. Meteor. Soc. Japan*, **82**, 1577–1588, doi: 10.2151/jmsj.82.1577.

Wallace, J. M., and D. S. Gutzler, 1981: Teleconnections in the geopotential height field during the Northern Hemisphere winter. *Mon. Wea. Rev.*, **109**, 784–812, doi: 10.1175/1520-0493(1981)109<0784:TITGHF<2.0.CO;2.

Wang, H., B. Wang, F. Huang, et al., 2012: Interdecadal change of the boreal summer circumglobal teleconnection (1958–2010). *Geophys. Res. Lett.*, **39**, L12704, doi: 10.1029/2012GL052371.

Wang, L., and W. Chen, 2014: An intensity index for the East Asian winter monsoon. *J. Climate*, **27**, 2361–2374, doi: 10.1175/JCLI-D-13-00086.1.

Wang, L. J., C. Wang, and D. Guo, 2018: Evolution mechanism of synoptic-scale EAP teleconnection pattern and its relationship to summer precipitation in China. *Atmos. Res.*, **214**, 150–162, doi: 10.1016/j.atmosres.2018.07.023.

Wang, N., and Y. C. Zhang, 2015: Connections between the Eurasian teleconnection and concurrent variation of upper-level jets over East Asia. *Adv. Atmos. Sci.*, **32**, 336–348, doi: 10.1007/s00376-014-4088-1.

Wen, M., S. Yang, A. Kumar, et al., 2009: An analysis of the large-scale climate anomalies associated with the snowstorms affecting China in January 2008. *Mon. Wea. Rev.*, **137**, 1111–1131, doi: 10.1175/2008MWR2638.1.

Yang, R. W., Y. Tao, and J. Cao, 2010: A mechanism for the interannual variation of the early summer East Asia–Pacific teleconnection wave train. *Acta Meteor. Sinica*, **24**, 452–458.

Zhou, T. J., B. Wu, and B. Wang, 2009: How well do atmospheric general circulation models capture the leading modes of the interannual variability of the Asian–Australian Monsoon? *J. Climate*, **22**, 1159–1173, doi: 10.1175/2008jcli2245.1.

Zhou, W., J. C. L. Chan, W. Chen, et al., 2009: Synoptic-scale controls of persistent low temperature and icy weather over southern China in January 2008. *Mon. Wea. Rev.*, **137**, 3978–3991, doi: 10.1175/2009MWR2952.1.

Tech & Copy Editor: Meili ZHANG